Applied Physics Letters

High-resolution virtual Frisch grid gamma-ray detectors based on as-grown CdZnTeSe with reduced defects

Cite as: Appl. Phys. Lett. **114**, 232107 (2019); https://doi.org/10.1063/1.5109119
Submitted: 06 May 2019 . Accepted: 03 June 2019 . Published Online: 14 June 2019

Utpal N. Roy, Giuseppe S. Camarda, Yonggang Cui, and Ralph B. James

Applied Physics Letters ARTICLE scitation.org/journal/apl

High-resolution virtual Frisch grid gamma-ray detectors based on as-grown CdZnTeSe with reduced defects

Cite as: Appl. Phys. Lett. **114**, 232107 (2019); doi: 10.1063/1.5109119
Submitted: 6 May 2019 · Accepted: 3 June 2019 ·
Published Online: 14 June 2019

Utpal N. Roy,[a] Giuseppe S. Camarda, Yonggang Cui, and Ralph B. James[b]

AFFILIATIONS

Brookhaven National Laboratory, Upton, New York 11973, USA

[a]**Author to whom correspondence should be addressed:** uroy@bnl.gov
[b]**Present address:** Savannah River National Laboratory, Aiken, SC 29808, USA.

ABSTRACT

X- and gamma-ray detectors are increasingly becoming essential tools for science and technology in various fields. These detectors offer broad applications such as homeland security, nonproliferation, nuclear security, medical imaging, astrophysics, and high energy physics. All these applications demand high-resolution detectors operable at room temperature and available at a reasonable cost. CdZnTe (CZT) is the material of choice for this purpose; however, the material still suffers from intrinsic defects such as highly decorated subgrain boundary networks and a high concentration of secondary phases. These defects not only hinder the charge transport but also create a spatial inhomogeneity in the charge transport properties, subsequently causing substantial degradation in detector response particularly for relatively thick (>1 cm) detectors. Some of the material deficiencies suffered by CZT have been addressed by adding selenium into the CZT matrix. Selenium was found to be very effective in producing material that is principally free from a subgrain boundary network with the occasional appearance of subgrain boundaries with reduced secondary phases decorating these boundaries. The resulting quaternary compound CdZnTeSe (CZTS) showed excellent material quality mitigating some major deficiencies suffered by CZT. Virtual Frisch grid detectors were fabricated from the as-grown CZTS ingots, and they demonstrated high resolution spectroscopic grade. The excellent CZTS material contained very low defects and was found to potentially increase the yield of high-quality detectors as compared to CZT.

Over four decades of intense global research has been dedicated to the identification of room-temperature semiconductor X- and gamma-ray detector materials. Despite these efforts, $Cd_{0.9}Zn_{0.1}Te$ (CZT) still dominates the commercial market due to its favorable physical and optoelectronic properties. The quality of the CZT material and its charge transport properties have been continuously improving through this extensive development period.[1–7] However, despite many years of research and development, CZT still suffers from the occurrence of a large concentration of detrimental defects, such as subgrain boundary networks and a high concentration of secondary phases commonly known as Te inclusions. These defects cause severe degradation of the detector response.[8–10] Because of the random distribution of subgrain boundary networks in the CdTe/CZT matrix, these defects are also responsible for an inhomogeneous spatial distribution of trapping centers, which causes spatial variability in the charge transport properties throughout the active volume of CZT devices. These variations can severely degrade the energy resolution of the detectors, especially for thick (less than about 1 cm) detectors, which are required for detecting hard X-rays and gammas.[11]

These Te inclusions act as major trapping centers and severely hinder the charge transport beyond their actual size.[12] The mobility-lifetime product for electrons $[(\mu\tau)_e]$ was reported to vary over a large range of between 0.2 and 20×10^{-3} cm^2/V for the region with high inclusions compared to the clear regions that are free of large inclusions.[9] This spatial variation of charge transport properties is responsible for producing different pulse heights in the detectors and eventually degrading the spectroscopic performance of the detector.[10,12]

The subgrain boundaries and their network in CZT are also known to be heavily decorated with Te inclusions.[8] Although it is a common practice in industry to use postgrowth annealing in a Cd vapor to eliminate the Te inclusions, the process produces starlike defects that are typically 50–100 times larger than the actual Te inclusion. These starlike defects are invisible to common inspection methods relying on infrared (IR) transmission. They also act as trapping

centers and severely hinder the charge transport for electron clouds that impinge on one of these extended defects.[13] Thus, a stringent material requirement and key to increasing the yield of high-quality detectors is to produce material with high spatial uniformity in the charge transport properties. For CZT and related compounds, this requires a reduction in the concentration and size of Te inclusions in the crystals and an absence of subgrain boundary networks and star-like defects.

In the present report, we made an effort to reduce the abovesaid defects by adding selenium to the CZT matrix and characterize the detectors fabricated from as-grown $Cd_{0.9}Zn_{0.1}Te_{0.98}Se_{0.02}$ by the Traveling Heater Method (THM).

CZTS ingots with a 2-in. diameter were grown by THM using 6N purity Te from Alfa Aesar as the solvent. The $Cd_{0.9}Zn_{0.1}Te_{0.98}Se_{0.02}$ material was synthesized from 6N purity $Cd_{0.9}Zn_{0.1}Te$ and 6N purity CdSe, procured from 5N Plus, Inc. and Azelis, Inc., respectively. Growth conditions for CZT were reported in an earlier manuscript,[14] and these conditions were adapted by the authors to grow the $Cd_{0.9}Zn_{0.1}Te_{0.98}Se_{0.02}$ ingots used in this study.

Detectors were fabricated in a virtual Frisch grid (VFG) geometry using samples cut from the as-grown CZTS ingots. The detectors were cut from unknown randomly oriented single crystalline grains. The virtual Frisch grid geometry detectors are simple and effective electron-only devices. The VFG devices are large geometrical aspect ratio parallelepiped bar shaped detectors, with the two end faces being metalized and acting as the anode and the cathode. The side walls are wrapped with an insulating layer, followed by wrapping with a metallic layer of aluminum or copper which acts as a Frisch grid. Teflon, Kapton tape, or thin polyester layers are often used as an insulating layer between the crystal wall and the Frisch grid.[15–18] Fabrication of virtual Frisch grid detectors and their operating principles are detailed in the literature.[15–20] A programable diamond-impregnated wire saw was used for cutting. The detector samples were lapped with successive grit-size SiC paper and finally polished to a mirror finish using 0.05-μm size alumina suspension on a felt pad. The presence of Te-rich secondary phases (i.e., inclusions) was studied by infrared (IR) transmission microscopy using a Nikon, Eclipse LV 100 Microscope at different magnifications. White Beam X-ray Diffraction Topography (WBXDT) measurements were carried out in the reflection mode to study the subgrain boundaries and their network. The WBXDT measurements were conducted at LBNL's ALS Beamline 3.3.2 with an X-ray beam energy ranging from 4 to 25 keV. Prior to the X-ray topographic measurements, the samples were etched in freshly prepared 2% bromine-methanol (BM) solution for two minutes to remove the damaged layer created during the surface polishing process. Detectors were fabricated on polished surfaces only (i.e., no bromine-methanol etch), and electroless gold contacts were deposited from a gold chloride solution on the cathode and anode sides. We preferred to fabricate the detectors on the polished surface to reduce the leakage current, and the BM etched surface showed higher leakage current. A point gamma radiation source was placed on the cathode side for all the detector measurements. The induced signal was measured through an electronvolt product A 4039 preamplifier and an Ortec 672 shaping amplifier, and MCA-3 series/P 7882 card from FAST ComTec. was used to register the spectra. The shaping time used for all the spectra was 2 μs. All the detector measurements were carried out at room temperature (~21–23 °C).

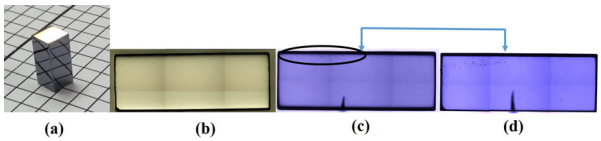

FIG. 1. Detector #1: (a) Optical photograph of the virtual Frisch grid detector sample with gold contacts, (b) optical scanning microscopy image of the detector in the reflection mode and (c) in the IR transmission mode, and (d) IR transmission image observed through the upper surface of (c). The detector dimensions: $5 \times 5 \times 12.3\,mm^3$.

The CZTS ingots are large-grain polycrystalline in nature, and the largest grain area was $\sim 2.5 \times 1.75\,cm^2$. The dark resistivity at room temperature was found to be in the range of $1–3 \times 10^{10}\,\Omega\,cm$. The highest mobility-lifetime product for electrons $(\mu\tau)_e$ was found to be $\sim 6.5 \times 10^{-3}\,cm^2/V$; however, the average $(\mu\tau)_e$ value for the CZTS samples was between 4 and $5 \times 10^{-3}\,cm^2/V$. The $(\mu\tau)_e$ values were estimated by Hecht fitting of the charge collection vs applied bias curve for planar detectors.[14,21]

Frisch grid detectors fabricated from the as-grown CZTS ingot were evaluated by infrared transmission microscopy, X-ray topography, and detector performance characteristics. The optical photographs of two detector samples with gold contacts fabricated from the as-grown CZTS ingot are shown in Figs. 1(a) and 2(a). The scanning microscopy images of the two detectors in reflection and IR transmission modes are illustrated in Figs. 1(b) and 1(c) and 2(b) and 2(c) for the two detectors, respectively. As is evident from Figs. 1(c) and 2(c), very few Te inclusions are present in the as-grown samples. To evaluate in more detail, high-magnification IR transmission microscopy studies were carried out. Figures 3(a)–3(d) show high-magnification IR transmission microscopy images with successive increased magnifications.

The high-magnification IR transmission images illustrate the presence of very few Te inclusions present in the as-grown CZTS samples. In some regions, however, we observed relatively large Te inclusions with a size of ~14–20 μm at a very low concentration; a typical hexagonal Te inclusion observed by IR microscopy is shown in Fig. 4. The presence of large Te inclusions was observed as indicated by the ellipse in the photograph of detector #1 [see Fig. 1(c)]. These inclusions were observed to be along the length of the detector at a depth below the sample surface. The IR transmission view from the top of the surface of Fig. 1(c) is shown in Fig. 1(d), showing the presence of large Te inclusions. These inclusions are possibly due to a localized instability at the growth interface, resulting in Te entrapment at the interface. The occurrence of such large Te inclusions is common for THM-grown CZT.[22]

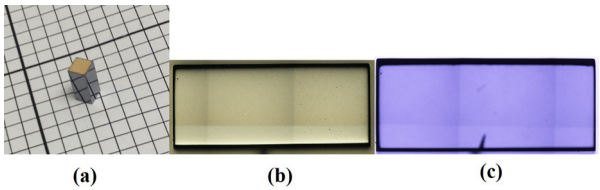

FIG. 2. Detector #2: (a) Optical photograph of the virtual Frisch grid detector sample with gold contacts and (b) optical scanning microscopy image of the detector in the reflection mode and (c) in the IR transmission mode. The detector dimensions: $4.5 \times 4.5 \times 10.8\,mm^3$.

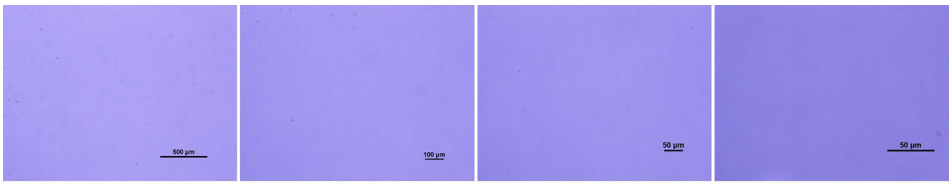

FIG. 3. High-magnification IR transmission microscopy image with increased magnification from left to right.

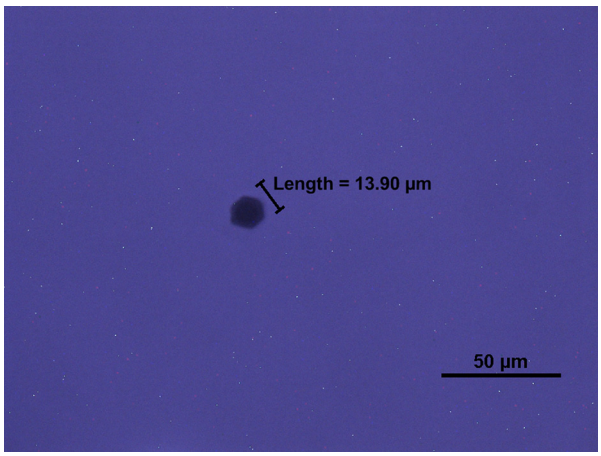

FIG. 4. High-magnification IR transmission microscopy images of an as-grown CZTS sample showing a hexagonal Te inclusion.

X-ray topographic analyses revealed the absence of subgrain boundary network for all the CZTS samples. In general, CZT samples are reported to be highly decorated with subgrain boundary networks.[8] In the reflection mode, X-ray topography reveals the subgrain boundary and their network by the appearance of white and dark lines. The white lines correspond to the separation of the diffracted images of the adjacent subgrains, while the dark lines correspond to the overlap of the diffracted images depending on the crystallographic tilt of the adjacent subgrains. The left side of Figs. 5 and 6 illustrates the X-ray topographic image of the two detectors. A prominent subgrain boundary is evident as marked by the black arrows in Fig. 6, while no subgrain boundary was detected for detector #1 as shown in Fig. 5. For both the samples, unlike CZT, no subgrain boundary network was observed. A few scratches are visible as marked by the blue arrows in Figs. 5 and 6. Selenium was thus found to be very effective as a solid solution hardening agent to arrest the formation of subgrain boundary networks. Selenium has long been known to be effective in producing subgrain boundary free CdTeSe (CTS) ingots with Se atomic concentrations as low as 0.4%.[23] We also observed a similar effect for THM-grown $CdTe_{0.9}Se_{0.1}$ and $Cd_{0.9}Zn_{0.1}Te_{0.93}Se_{0.07}$ ingots.[24,25] It is thus evident from IR microscopy and X-ray topography experiments that the Te inclusions and subgrain boundary and their network are significantly reduced by the presence of Se in the as-grown CZTS samples.

The detector responses for the 662-keV gamma line from a ^{137}Cs source for the two virtual Frisch grid detectors are shown in Figs. 5 and 6. High resolution spectroscopic performances were achieved for both the detectors. Energy resolutions of ∼0.9% and ∼1.08% at 662 keV were obtained for detector #1 and detector #2, under the applied bias of 1800 V and 3000 V, respectively. The resolution of the electronic pulse shown in Fig. 5 is ∼0.6%. It is noted that some low-energy tailing is observed for detector 1 (see Fig. 5). We believe that the presence of large Te inclusions along the length of the detector [indicated in Fig. 1(c)] is responsible for this low energy tailing. We have studied many Frisch grid detectors fabricated from the as-grown CZTS ingot, and no detector showed as much low energy tailing, as shown in Fig. 6 for detector #2. We also noticed higher dark current for detector #1 at an applied bias of 500 V as compared to detector #2.

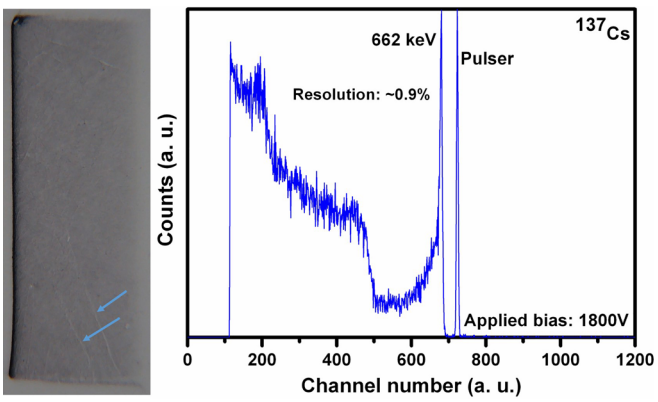

FIG. 5. Detector #1: X-ray topographic image of the whole detector (left) and the pulse height spectrum of the virtual Frisch grid detector for a ^{137}Cs source at room temperature. Blue arrows indicate scratches on the sample surface.

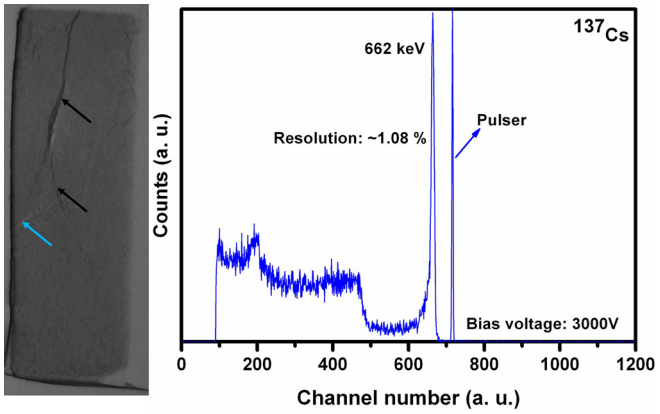

FIG. 6. Detector #2: X-ray topographic image of the whole detector (left) and the pulse height spectrum of the virtual Frisch grid detector at room temperature for a ^{137}Cs source. The blue arrow indicates a scratch on the sample surface, while the black arrows indicate a subgrain boundary.

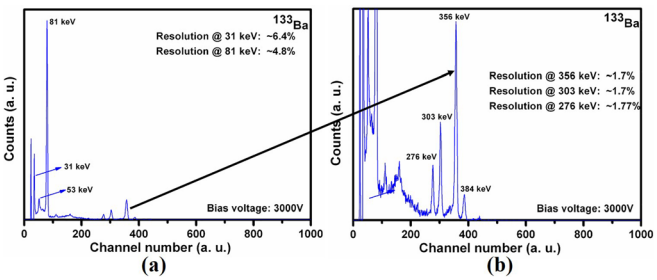

FIG. 7. Detector #2: Pulse height spectrum of the virtual Frisch grid detector for the ^{133}Ba source at room temperature.

The higher dark current for detector #1 might be due to the Te-inclusions along one of the side walls. The dark currents for detector #1 and detector #2 were found to be 1 nA and 0.7 nA, respectively, under the bias of 500 V. It is apparent from Figs. 5 and 6 that the absence of any subgrain boundary for detector #1 (Fig. 5) yields better energy resolution at 662 keV, under a much lower applied electric field. The higher operating voltage for detector #2, as well as relatively worst energy resolution compared to detector #1, might be due to the deleterious effect of the subgrain boundary present in detector #2. The detectors also showed a very high resolution at low energy gammas. The pulse height spectrum from detector #2 for the ^{133}Ba source is shown in Fig. 7(a), depicting very well resolved lines with a high energy resolution. The obtained energy resolutions at 31 keV and 81 keV were ∼6.4% and 4.8%, respectively. Figure 7(b) shows a magnified version of Fig. 7(a) to enhance visualization of the peaks in the range of 276 keV and 384 keV. As indicated in Fig. 7(b), the energy resolutions were ∼1.7%, 1.7%, and ∼1.8% for 356 keV, 303 keV, and 276 keV gamma lines, respectively. All the spectra demonstrated here were recorded on as-measured detectors (i.e., no pulse processing to correct for charge trapping), and the detectors were fabricated from the as-grown CZTS ingots (i.e., no postgrowth thermal annealing). The spectra illustrated in this report were taken at room temperature (∼21–23 °C).

In this paper, we showed that quaternary CZTS can be grown free from subgrain boundary networks with a very low relative content of Te inclusions, as compared to CZT (without Se). High-quality spectroscopic grade virtual Frisch grid detectors fabricated from as-grown CZTS demonstrate excellent material properties. The increased uniformity manifested by the absence of a subgrain boundary network and the reduced density of Te-rich secondary phases in CZTS show that the quaternary material is a very promising candidate for increasing the yield of high-quality detectors.

This work was supported by the U.S. Department of Energy, Office of Defense Nuclear Nonproliferation Research and Development, DNN R&D. This manuscript was authored by Brookhaven Science Associates, LLC, under Contract No. DE-SC0012704 with the U.S. Department of Energy.

REFERENCES

[1]T. E. Schlesinger, J. E. Toney, H. Yoon, E. Y. Lee, B. A. Brunett, L. Franks, and R. B. James, Mater. Sci. Eng. R **32**, 103 (2001).
[2]G. Yang and R. B. James, in *Physics, Defects, Hetero- and Nano-Structures, Crystal Growth, Surfaces and Applications: Part II, EDAX*, edited by R. Triboulet *et al.* (Elsevier, 2009), p. 214.
[3]A. El Mokri, R. Triboulet, A. Lusson, A. Tromson-Carli, and G. Didier, J. Cryst. Growth **138**, 1 (1994).
[4]A. Burger, M. Groza, Y. Cui, U. N. Roy, D. Hillman, M. Guo, L. Li, G. W. Wright, and R. B. James, Phys. Status Solidi C **2**, 1586 (2005).
[5]H. Chen, S. A. Awadalla, F. Harris, P. Lu, R. Redden, G. Bindley, A. Copete, J. Hong, J. Grindlay, M. Amman, J. S. Lee, P. Luke, I. Kuvvetli, and C. Budtz-Jorgensen, IEEE Trans. Nucl. Sci. **55**, 1567 (2008).
[6]J. Mackenzie, F. J. Kumar, and H. Chen, J. Electron. Mater. **42**, 3129 (2013).
[7]H. Chen, H. Li, M. D. Reed, A. G. Sundaram, J. Eger, J. W. Hugg, S. Abbaszadeh, M. Li, G. Montemont, L. Verger, Y. Zhu, and Z. He, Proc. SPIE **10762**, 107620N (2019).
[8]A. E. Bolotnikov, G. S. Camarda, Y. Cui, G. Yang, A. Hossain, K. Kim, and R. B. James, J. Cryst. Growth **379**, 46 (2013).
[9]G. A. Carini, A. E. Bolotnikov, G. S. Camarda, and R. B. James, Nucl. Instrum. Methods Phys. Res., Sect. A **579**, 120 (2007).
[10]A. E. Bolotnikov, G. S. Camarda, G. A. Carini, Y. Cui, K. T. Kohman, L. Li, M. B. Salomon, and R. B. James, IEEE Trans. Nucl. Sci. **54**, 821 (2007).
[11]A. E. Bolotnikov, K. Ackley, G. S. Camarda, Y. Cui, J. F. Eger, G. De Geronimo, C. Finfrock, J. Fried, A. Hossain, W. Lee, M. Prokesch, M. Petryk, J. L. Reiber, U. Roy, E. Vernon, G. Yang, and R. B. James, IEEE Trans. Nucl. Sci. **62**, 3193 (2015).
[12]M. Amman, J. S. Lee, and P. N. Luke, J. Appl. Phys. **92**, 3198 (2002).
[13]G. Yang, A. E. Bolotnikov, P. M. Fochuk, O. Kopach, J. Franc, E. Belas, K. H. Kim, G. S. Camarda, A. Hossain, Y. Cui, A. L. Adams, A. Radja, R. Pinder, and R. B. James, J. Cryst. Growth **379**, 16 (2013).
[14]U. N. Roy, A. Gueorguiev, S. Weiller, and J. Stein, J. Cryst. Growth **312**, 33 (2009).
[15]W. J. McNeil, D. S. McGregor, A. E. Bolotnikov, G. W. Wright, and R. B. James, Appl. Phys. Lett. **84**, 1988 (2004).
[16]A. Kargar, A. M. Jones, W. J. McNeil, M. J. Harrison, and D. S. McGregor, Nucl. Instrum. Methods Phys. Res., Sect. A **558**, 497 (2006).
[17]G. Montémont, M. Arques, L. Verger, and J. Rustique, IEEE Trans. Nucl. Sci. **48**, 278 (2001).
[18]A. E. Bolotnikov, J. Butcher, G. S. Camarda, Y. Cui, G. De Geronimo, J. Fried, R. Gul, P. M. Fochuk, M. Hamade, A. Hossain, K. H. Kim, O. V. Kopach, M. Petryk, E. Vernon, G. Yang, and R. B. James, IEEE Trans. Nucl. Sci. **59**, 1544 (2012).
[19]D. S. McGregor, Z. He, H. A. Seifert, R. A. Rojeski, and D. K. Wehe, IEEE Trans. Nucl. Sci. **45**, 443 (1998).
[20]D. S. McGregor and R. A. Rojeski, U.S. patent 6,175,120 (16 January 2001).
[21]U. N. Roy, S. Weiler, J. Stein, M. Groza, V. Buliga, and A. Burger, Nucl. Instrum. Methods Phys. Res., Sect. A **652**, 162 (2011).
[22]U. N. Roy, S. Weiller, and J. Stein, J. Cryst. Growth **312**, 2840 (2010).
[23]P. Rudolph, Prog. Cryst. Growth Charact. Mater. **29**, 275 (1994).
[24]U. N. Roy, A. E. Bolotnikov, G. S. Camarda, Y. Cui, A. Hossain, K. Lee, G. Yang, and R. B. James, J. Cryst. Growth **389**, 99 (2014).
[25]U. N. Roy, G. S. Camarda, Y. Cui, R. Gul, A. Hossain, G. Yang, J. Zazvorka, V. Dedic, J. Franc, and R. B. James, Sci. Rep. **9**, 1620 (2019).